Journal of Nanobiotechnology

RESEARCH Open Access

Noninvasive molecular imaging using anti-Trop-2 aptamer for targeted therapy of small cell lung cancer

Yamei Chen[1†], Xuwei Liu[2†], Yang Sun[1†], Keying Liu[1], Ding Ding[1*], Shaoli Song[2*] and Weihong Tan[1,3*]

Abstract

Recent advancements in antibody-drug conjugates (ADCs) targeting trophoblast surface cell antigen 2 (Trop-2) have brought important progress in the field of targeted therapy. This progress also holds promise for the treatment of small cell lung cancer (SCLC) as anti-Trop-2 therapy appears to have a safe and effective clinical activity in metastatic SCLC patients. However, effective treatments of anti-Trop-2 ADCs rely on the comprehensive assessment of Trop-2 expression at the tumor sites, SCLC exhibits intratumoral heterogeneity, making the accurate acquisition of histological biopsies a challenge. To address this issue, we herein report the development of an anti-Trop-2 aptamer consisting of 76 bases is specifically bind to Trop-2-overexpressing SCLC cells. Further truncated anti-Trop-2 aptamer with 46 nucleotides also possesses excellent in vitro and in vivo binding affinity with Trop-2 antigens. After radiolabeling with gallium-68 radionuclide, an aptamer-based molecular imaging probe was successfully fabricated named [^{68}Ga]Ga-NOTA-TRP-c. This imaging probe demonstrated effective and precise differentiation of Trop-2-positive tumors in both murine- and human-derived animal models, exhibiting favorable metabolic profiles. Furthermore, Trop-2-positive SCLC tumors recognized by anti-Trop-2 aptamer can be treated with anti-Trop-2 ADC sacituzumab govitecan (SG), either in vitro or in vivo. Importantly, SG induces DNA damage and cell apoptosis without affecting the expression of Trop-2 on the cell surface, which makes it possible to use anti-Trop-2 aptamer to monitor the expression of Trop-2 in SCLC. This study highlights the potential of aptamer-based molecular imaging and imaging-guided SG treatment as a promising option for targeted therapy in SCLC.

Keywords Small cell lung cancer, Trop-2, Aptamer, Molecular imaging, Antibody-drug conjugates

Introduction

Lung cancer is the primary cause of cancer-related mortality globally with a projected 125,070 deaths in the United States in 2024 [1]. Small cell lung cancer (SCLC), a distinct pathological and clinical subtype, represents about 15% of lung cancer patients, and it is characterized by exceptionally aggressive proliferation and poor prognosis [2]. Most patients with SCLC are diagnosed at an advanced stage, limiting treatment options [3, 4]. Current treatment involves chemotherapy and radiotherapy, but recurrent and chemoresistant disease is common, leading to short survival times [2, 5]. Besides, no targeted

†Yamei Chen, Xuwei Liu and Yang Sun contributed equally to this work.

*Correspondence:
Ding Ding
dding@sjtu.edu.cn
Shaoli Song
shaoli-song@163.com
Weihong Tan
tan@him.cas.cn

Full list of author information is available at the end of the article

© The Author(s) 2025. **Open Access** This article is licensed under a Creative Commons Attribution-NonCommercial-NoDerivatives 4.0 International License, which permits any non-commercial use, sharing, distribution and reproduction in any medium or format, as long as you give appropriate credit to the original author(s) and the source, provide a link to the Creative Commons licence, and indicate if you modified the licensed material. You do not have permission under this licence to share adapted material derived from this article or parts of it. The images or other third party material in this article are included in the article's Creative Commons licence, unless indicated otherwise in a credit line to the material. If material is not included in the article's Creative Commons licence and your intended use is not permitted by statutory regulation or exceeds the permitted use, you will need to obtain permission directly from the copyright holder. To view a copy of this licence, visit http://creativecommons.org/licenses/by-nc-nd/4.0/.

Graphical Abstract

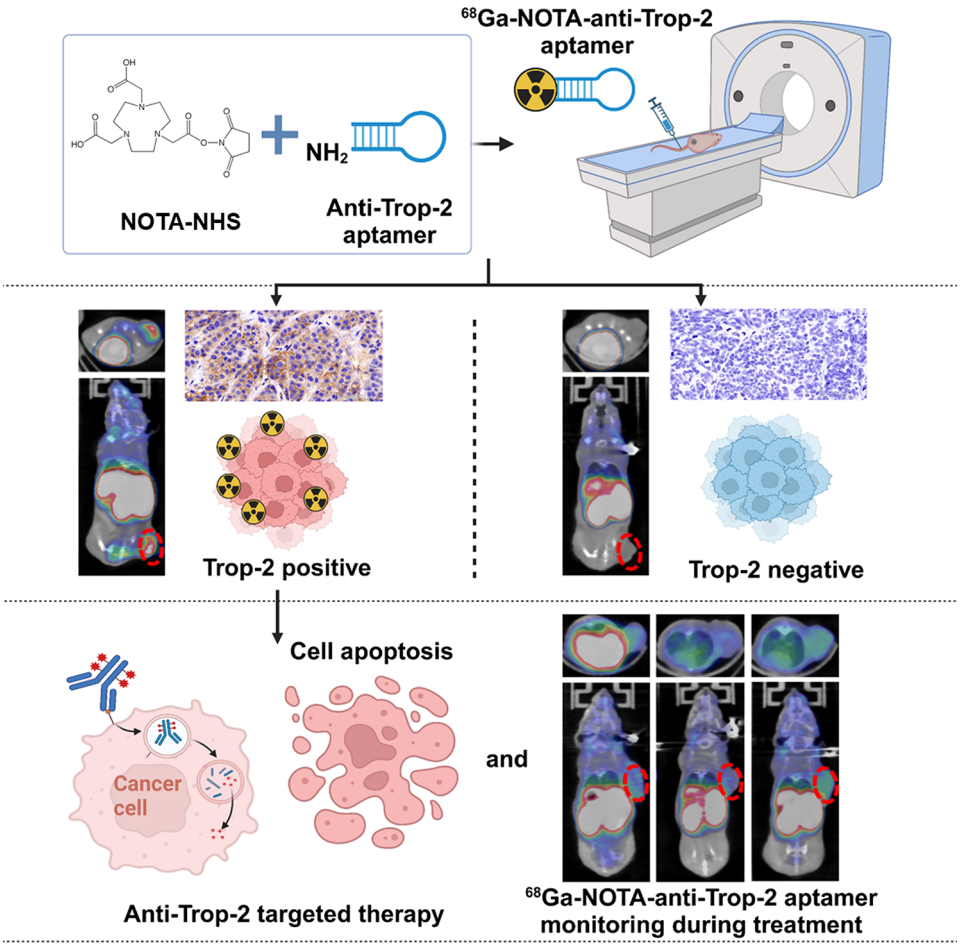

therapies are currently available for patients with SCLC, and only a small subset of patients benefits from the use of immune checkpoint inhibitors [6, 7]. The identification of molecular targets for the rational design of more durably effective therapies is a major unmet clinical need. Trophoblast surface cell antigen 2 (Trop-2) is a surface glycoprotein member of the epithelial cell adhesion molecule (EpCAM) family, and it is overexpressed in a wide variety of epithelial tumors, including lung cancer [8, 9]. High expression level of Trop-2 is associated with poor prognosis and the regulation of cell proliferation and metastasis in lung cancer [10–13]. The recent advancement in anti-Trop-2 antibody-drug conjugates (ADCs), specifically sacituzumab govitecan (SG), an anti-Trop-2 antibody linked to the topoisomerase I inhibitor SN38 warhead, has shown notable success in treating metastatic triple-negative breast cancer (TNBC). In SCLC, clinical trials [14, 15] evaluating the efficacy of SG have been conducted, yet the overall response rate (ORR) of SG in these trials is not ideal, necessitating further studies, either as a monotherapy or combination therapy. Since results from the ASCENT test showed that SG doubled the ORR and progression-free survival (PFS) in TNBC patients with high or moderate expression of Trop-2, the overall expression level of Trop-2 in the tumor region might determine the therapeutic effectiveness of SG [16]. Hence, a comprehensive evaluation and analysis of Trop-2 expression could help identify SCLC patients most likely to benefit from SG therapy.

The conventional method of biomarker identification requires the acquisition of tissue samples from tumor lesions. However, patients with SCLC often lack surgical specimens, and diagnostic biopsy samples are usually limited in size and necrotic. In addition, obtaining repeated biopsy samples becomes challenging as the disease progresses. These clinical obstacles call for the development of novel detection methods for comprehensive and accurate assessment of Trop-2 expression levels in SCLC. Molecular imaging, particularly the recently developed immunoPET techniques, enables the in-situ

detection and assessment of disease-specific biomarkers through the use of radiolabeled targeting ligands, such as antibodies, peptides, aptamers, radiolabeled exosomes (EXOs) [17] and immune cells [18]. Among these targeting ligands, aptamers, typically a small fraction of DNA or RNA, have low immunogenicity, and they are amenable to chemical modification and bioconjugation compared to antibodies. The relatively small size and negative charges of aptamers allow for rapid tissue penetration and fast blood clearance to achieve high target-to-background ratio at early time points. Therefore, aptamers are promising candidates for molecular imaging and targeted therapy [19, 20]. For example, ^{18}F-labeled single-stranded DNA aptamer SGC8 has been reported to detect PTK7 expression in human colon cancer cell xenografted mice [21]. Tenascin-C aptamer was radiolabeled with ^{18}F and ^{64}Cu for PET imaging of human glioma and breast cancer cell-bearing nude mice [22]. Murine glioma was also successfully identified using ^{18}F-labeled complementary oligonucleotide, which hybridizes with nucleolin aptamer AS1411 [23]. Besides DNA aptamers, an ^{18}F-labeled RNA aptamer targeting EGFR has been studied in solid tumors [24]. Importantly, through in vivo PET tracking of gallium-68 (^{68}Ga)-radiolabeled SGC8 aptamer, our group reported the first-in-human dynamic pharmacokinetics study of aptamer [25], thereby establishing a solid foundation of aptamer-based molecular imaging for clinical translation. Numerous antibody-based imaging probes have been developed and utilized to target Trop-2 in pancreatic cancer and prostate cancer [26–30], yet, to the best of our knowledge, imaging probes based on aptamers are currently lacking. By harnessing the distinctive characteristics of aptamers, the development of an aptamer-based molecular imaging probe for the visualization and quantification of Trop-2 expression holds promise as a valuable tool for advancing precision medicine in SCLC.

In this study, an anti-Trop-2 DNA aptamer-based molecular imaging probe was developed for targeted imaging of Trop-2-positive SCLC tumors and imaging-guided targeted therapy. First, full-length anti-Trop-2 DNA aptamer consisting of 76 bases (TRPFL) was rationally developed, and then truncated with high specificity and moderate molecular weight for in vivo application (TRP-c). TRP-c exhibited specific binding capacity to Trop-2-overexpressing cells, as demonstrated in both human and murine SCLC cells with high levels of Trop-2 expression. Next, after radiolabeling of optimized anti-Trop-2 aptamer, we successfully fabricated an aptamer-based PET imaging probe and named it as [^{68}Ga]Ga-NOTA-TRP-c; this probe is capable of accurately evaluating Trop-2 expression in SCLC in vivo. The metabolic profile of this imaging probe was also studied, and quantification of its in vivo Trop-2 expression was carried out in mice bearing SBC-2, DMS 53, H446 and murine primary tumor cells RP-A21Lym in xenografts, all expressing different levels of Trop-2 antigens. Finally, [^{68}Ga]Ga-NOTA-TRP-c was applied to screen out SCLC cells with high Trop-2 expression. The Trop-2-positive SCLC cells and tumor animal models screened specifically by [^{68}Ga]Ga-NOTA-TRP-c were effectively eliminated upon treatment with the anti-Trop-2 ADC demonstrating the potential of anti-Trop-2 aptamer-based imaging-guided targeted therapy in SCLC.

Results

Heterogeneous expression of Trop-2 in small cell lung cancer

At present, emerging evidence suggests that SCLC exhibits substantial intertumoral and intratumoral heterogeneity in molecular expression at the protein level [31–33]. Therefore, we comprehensively evaluated the expression of Trop-2 in tumor tissues of patients with SCLC and in vitro cell lines.

In the paraffin-embedded surgical tumor samples from SCLC patients, Trop-2 was localized in the cytoplasm and cell membrane and was diffusely or locally overexpressed. Among these histology samples, about twelve tumors (22%) showed high and strong expression of Trop-2 protein, suggesting that these patients might benefit from anti-Trop-2 targeted therapy, and representative histopathological images are shown in Fig. 1A and SI Appendix, Fig. S1A. Furthermore, in vitro assessments were performed to study the difference between Trop-2 mRNA and protein expression levels among 4 human SCLC cell lines. As shown in Fig. 1B and SI Appendix, Fig. S1B and C, mRNA and whole protein expression levels of Trop-2 were higher in SBC-2 and DMS 53 cell lines in comparison with H446 and SW1271 cell lines. In addition, cell surface membrane Trop-2 proteins were also highly expressed in SBC-2 and DMS 53 compared to that in H446 and SW1271, as determined by flow cytometry and immunofluorescence assay, which is consistent with previous results (Fig. 1C and E and SI Appendix, Fig. S1D). Collectively, these results indicated that Trop-2 antigens were heterogeneously expressed and distributed in SCLC, may leading to ineffective therapy and lower-than-expected response rates in the absence of Trop-2-positive patient screening.

Optimization of the anti-Trop-2 aptamer for efficient targeting

Recently, our group designed a single-stranded anti-Trop-2 DNA aptamer containing 76 oligonucleotides (Molecular weight, MW = 23276.5 Da) (SI Appendix, Fig. S2A and B, Fig. S3A and B). This aptamer demonstrated excellent Trop-2 antigen binding affinity with 110.2 nM apparent dissociation constant (Kd) using surface

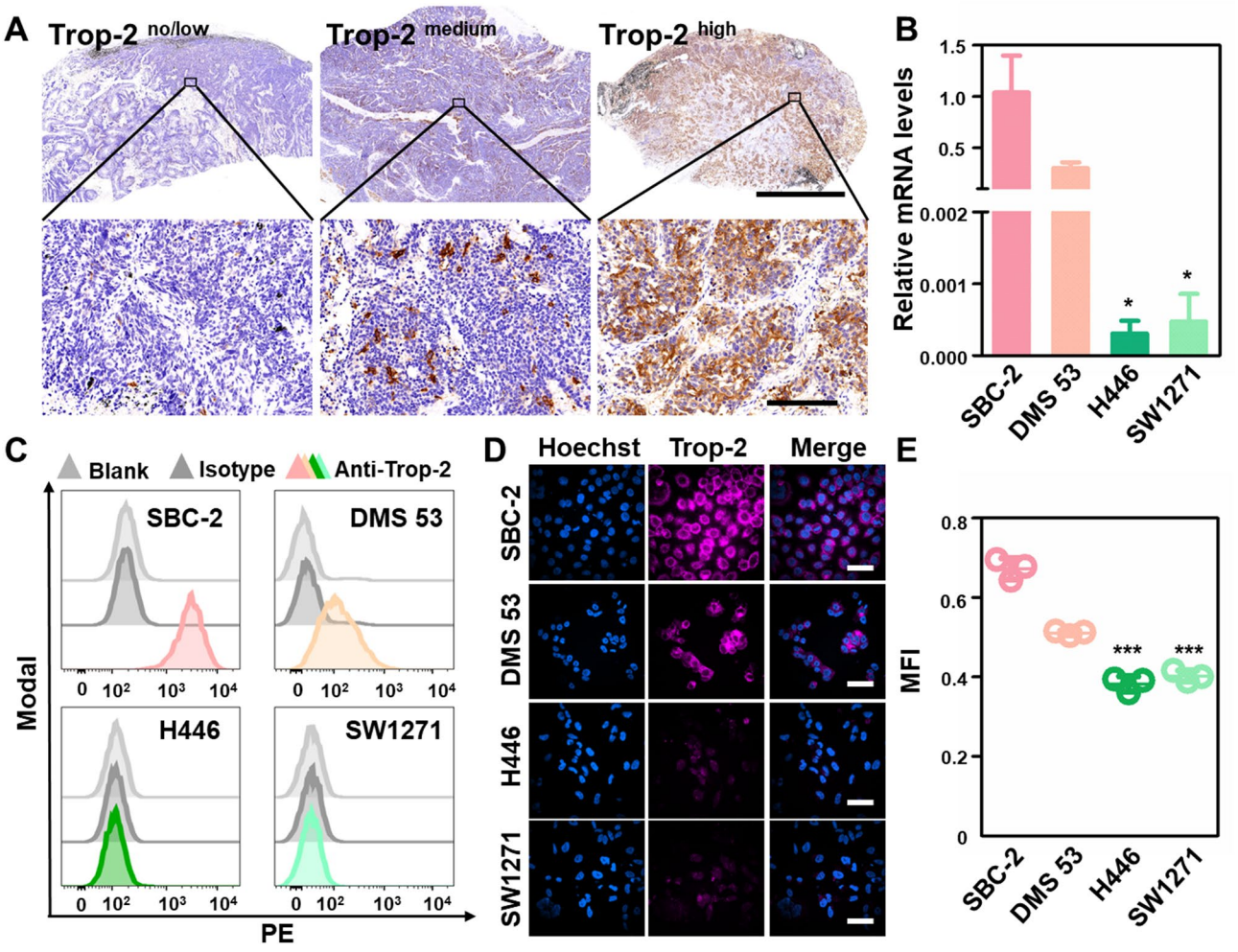

Fig. 1 Trop-2 expressed heterogeneously throughout the SCLC tumors and cells. (**A**) Representative immunohistochemical images of Trop-2 expression in human primary SCLC tumor samples. Scale bars, 2.5 mm and 100 μm. (**B**) Total mRNA expression levels of Trop-2 in four human SCLC cell lines. * represents versus SBC-2 cells $p < 0.05$. (**C**) Flow cytometry of cell membrane Trop-2 expression in four human SCLC cell lines. (**D**) Representative confocal images of cell surface and cytosolic Trop-2 in four human cell lines. Scale bars, 50 μm. (**E**) Quantitative analysis of Trop-2 protein level from data in (**D**). *** represents versus SBC-2 cells $p < 0.001$. Analyses were performed using unpaired, two-tailed Student's t test. Data are shown as means ± SD

plasmon resonance (SPR) (SI Appendix, Fig. S4A and B). To further reduce the cost of long nucleic acid synthesis, enhance functional feasibility, and improve biological stability, the full-length aptamer was truncated to TRP-a, TRP-b, TRP-c, and TRP-d. Sequences, MW and Kd value of these four truncated aptamers were presented in SI Appendix, Table 1, Fig. S2, Fig. S3 and Fig. S4. The stability of each aptamer in serum was evaluated using 10% FBS, followed by gel electrophoresis and quantitative analysis. As shown in SI Appendix Fig. S5A-B, more than 50% of the aptamers retained their integrity after 12 h incubation.

The binding affinities of full-length aptamer and its truncated variants were investigated on Trop-2-positive and -negative cells according to their surface protein expression levels. As shown in the fluorescence confocal microscopy analysis, the TRP-c sequence exhibited the best binding ability to Trop-2- positive SBC-2 cells (SI Appendix, Fig. S6A and B). Similar results were also validated through flow cytometry (FCM) (SI Appendix, Fig. S7A and B). Therefore, TRP-c showed the strongest binding affinity against Trop-2-positive SCLC cells, displaying a Kd of 87.83 ± 8.28 nM, as determined by FCM in SBC-2 cells (SI Appendix, Fig. S7C and D). Moreover, TRP-c exhibited enhanced cellular uptake by SBC-2 cells compared to the full-length sequence after prolonged incubation (SI Appendix, Fig. S8A and B). Next, we tested whether TRP-c aptamer staining could distinguish Trop-2-overexpressing cells from normal pulmonary epithelium and Trop-2-negative tumor cells. As expected, TRP-c could also bind to Trop-2-positive DMS 53 cells, while showing only minimal, to no, binding against normal Bease-2B cells and Trop-2-negative H446 cells (Fig. 2A and B, and SI Appendix, Fig. S9A-D). On the

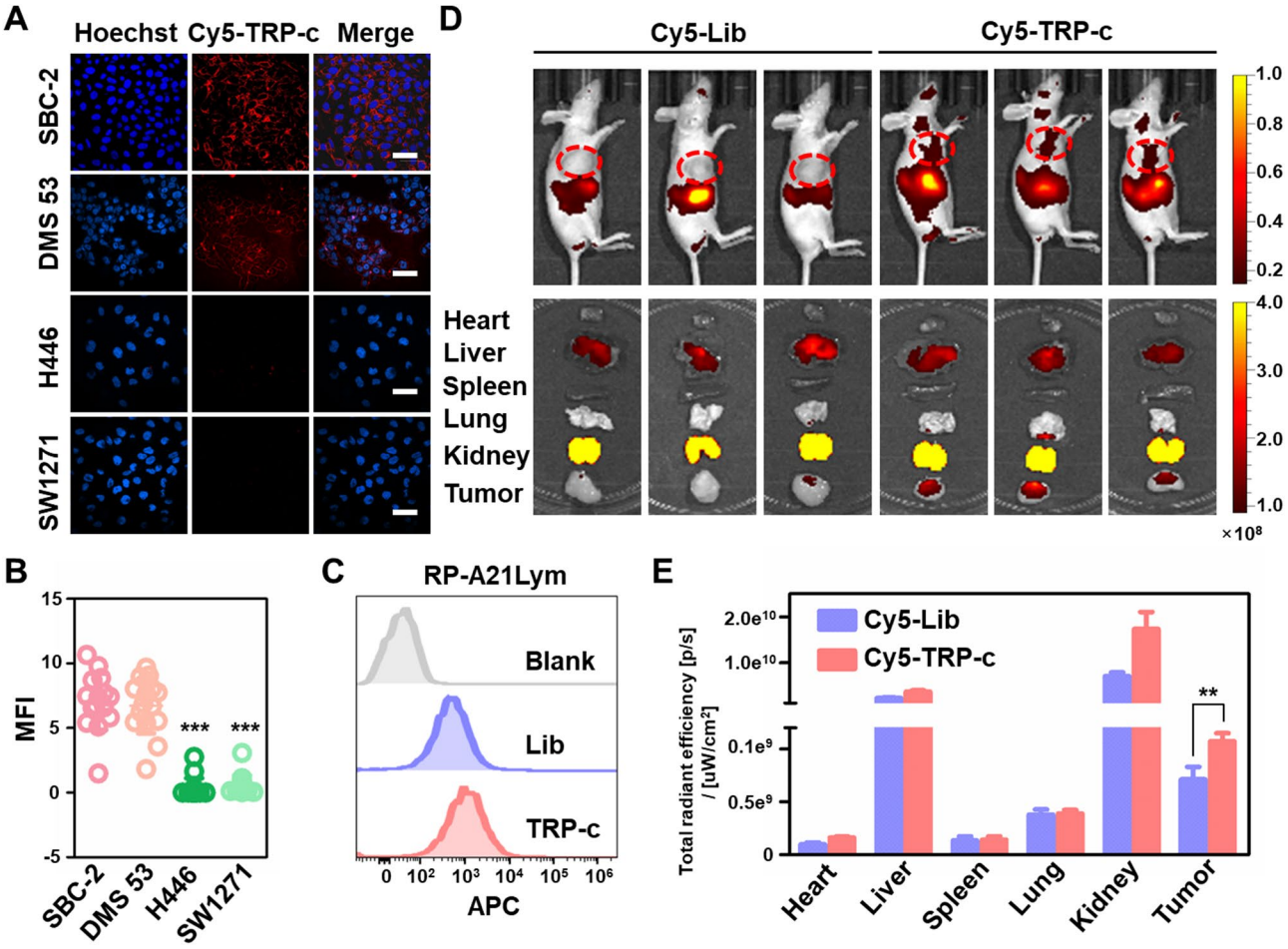

Fig. 2 Anti-Trop-2 aptamer specifically targeted SCLC. (**A**-**B**) Representative confocal images and quantification of Cy5-labeled anti-Trop-2 aptamer TRP-c targeting four human SCLC cell lines. Scale bars, 50 μm. (**C**) Binding ability of Cy5-labeled random sequence (Lib) and TRP-c to target primary mouse SCLC cells RP-A21Lym characterized by flow cytometry. (**D**) In vivo fluorescence imaging of RP-A21Lym cells in tumor-bearing BALB/c nude mice after random sequence Cy5-Lib or Cy5-TRP-c aptamer was injected intravenously. (**E**) Fluorescence imaging of biodistribution of Cy5-labeled random control sequence and TRP-c in ex vivo organs, including heart, liver, spleen, lung, kidney, and tumor after injection for 30 min, $n = 3$. ** represents $p < 0.01$. Tumor regions were labeled with red circles. Analyses were performed using unpaired, two-tailed Student's t test. Data are shown as means ± SD

other hand, human Trop-2 only shares 78.6% sequence identity with mouse Trop-2, resulting in variations in the binding capabilities of antibodies across species. Therefore, we also investigated the targeting ability of anti-Trop-2 aptamers in murine cells from $Trp53^{flox/flox}$; $Rb1^{flox/flox}$ mice at 8 months after Ad-Cre infection [34, 35]. Positive immunostaining of neuroendocrine (NE) markers Syn, CD56, CGRP and TTF-1 in RP-A21Lym cells confirmed that it originated from mouse SCLC (SI Appendix, Fig. S10). Consistent with human SCLC cells, TRP-c sequence showed more efficient targeting to RP-A21Lym cells compared to other sequences (Fig. 2C and SI Appendix, Fig. S11A and B). In contrast to antibodies, aptamers are sufficiently versatile to recognize both human and mouse targets, thus facilitating the further development of aptamer-based imaging probes and enabling the evaluation of effectiveness in various preclinical xenograft mouse models.

In addition, the in vivo targeting performance of TRP-c was studied in SBC-2 and RP-A21Lym mouse models. The targeted imaging of Trop-2-positive SCLC tumor models was achieved using Cyanine 5 (Cy5) fluorophore-labeled TRP-c, as depicted in Fig. 2D and SI Appendix, Fig. S12A. The results demonstrated obvious tumor accumulation of aptamers, and most of the aptamers were cleared from either kidney or liver (Fig. 2D and E, and SI Appendix, Fig. S12 B). In addition, single-cell suspensions were prepared from subcutaneous tumor specimens of mice bearing SBC-2 and RP-A21Lym after intravenous administration of Cy5-TRP-c, and FCM analysis showed that Cy5-TRP-c was significantly enriched in tumor cells (SI Appendix, Fig. S13A-D). Together, these results demonstrated that optimized aptamer TRP-c could recognize Trop-2 antigens on a variety of Trop-2-positive SCLC cell types and that it possesses the potential to be fabricated as a molecular imaging probe.

Preparation of [^{68}Ga]Ga-NOTA-TRP-c and pharmacokinetics study

To obtain an anti-Trop-2 aptamer-based PET imaging probe, TRP-c was coupled with a metal ion chelator, 1,4,7-triazacyclononane-1,4,7-triacetic acid (NOTA), and further labeled with ^{68}Ga radionuclide ($T_{1/2}$ = 1.1 h) (Fig. 3A). As previously reported, NOTA-TRP-c was synthesized by chemical coupling of the NH_2-TRP-c and NOTA-NHS via an amide bond [25]. After purification, NOTA-TRP-c displayed greater than 90% high performance liquid chromatography (HPLC). Further identification of NOTA-TRP-c was confirmed by electrospray ionization mass spectrometry (SI Appendix, Fig. S14A and B). The measured molecular weights of NH_2-TRP-c and NOTA-TRP-c match the calculated molecular weights. For radiolabeling, ^{68}Ga was eluted from a ^{68}Ge/^{68}Ga generator, and [^{68}Ga]Ga-NOTA-TRP-c was prepared with greater than 95% radiolabeling yield and 11.1–16.5 MBq/nmol specific activity. The final product was analyzed with radio-HPLC, and the retention time of [^{68}Ga]Ga-NOTA-TRP-c was 6.32–7.01 min (SI Appendix, Fig. S15A and B). The biological stability of radiolabeled TRP-c aptamer was studied, as depicted in SI Appendix Fig. S16A-B. Quantitative analysis revealed that [^{68}Ga]Ga-NOTA-TRP-c exhibited high stability in both serum and DPBS, with more than 80% of the radiolabeled aptamers retaining their integrity. Consistent with the electrophoresis results, PET imaging confirmed that most of the radioactivity of [^{68}Ga]Ga-NOTA-TRP-c remained intact within 2 h (SI appendix, Fig. S16C-D).

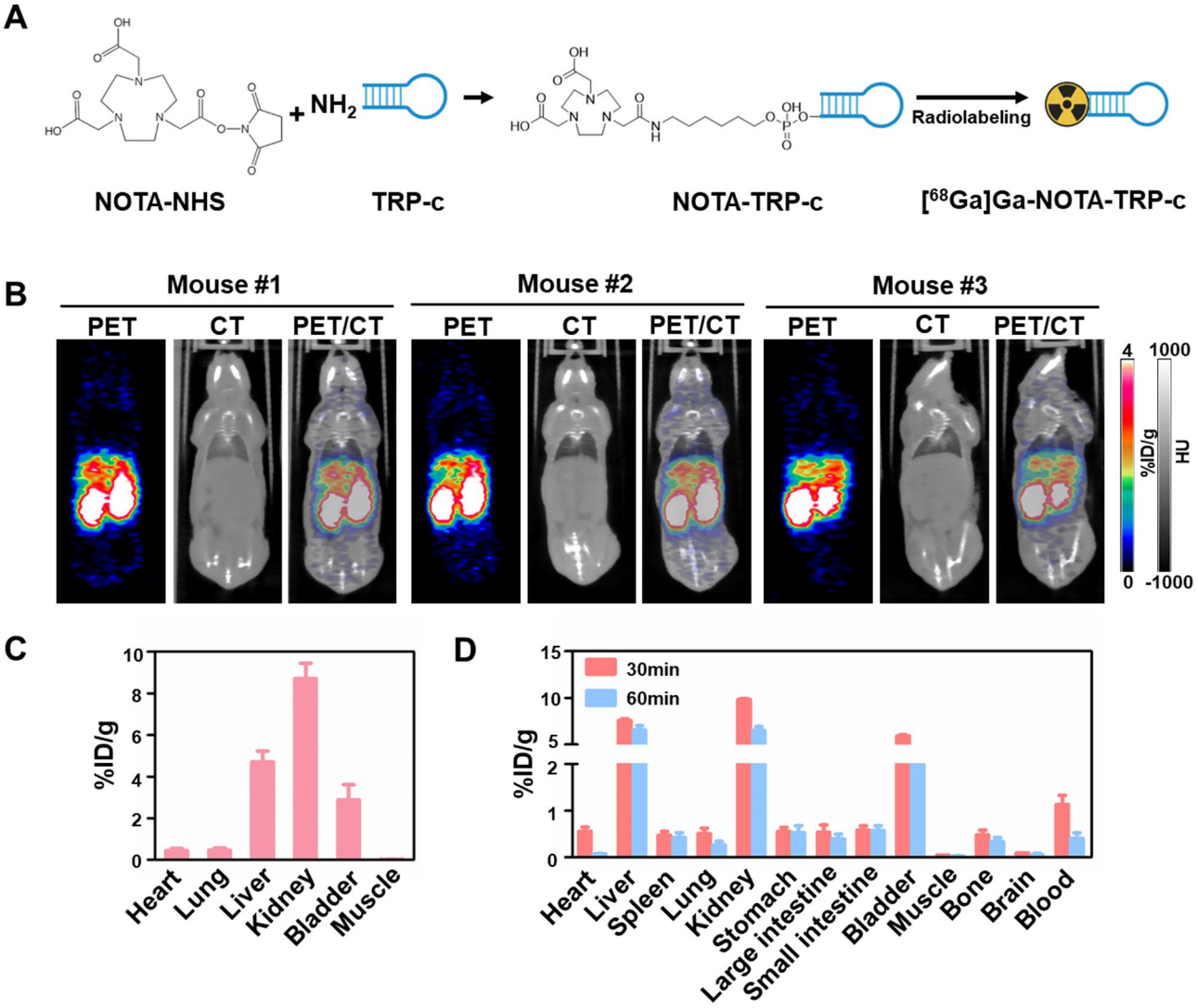

Fig. 3 Fabrication and pharmacokinetic studies of [^{68}Ga]Ga-NOTA-TRP-c aptamer in tumor-free Balb/c nude mice. (**A**) Schematic illustration of TRP-c aptamer radiolabeling. (**B**) [^{68}Ga]Ga-NOTA-TRP-c PET imaging in normal Balb/c nude mice at 30 min after injection. Coronal images showed clear delineation of kidneys and liver. (**C**) ROI analysis of PET imaging in tumor-free Balb/c nude mice at 30 min after injection of [^{68}Ga]Ga-NOTA-TRP-c ($n = 3$). (**D**) Radioactive biodistribution of [^{68}Ga]Ga-NOTA-TRP-c in tumor-free Balb/c nude mice 30 min ($n = 3$) and 60 min after injection ($n = 3$). HU, Hounsfield units

Circular dichroism (CD) spectrum characterization of anti-Trop-2 aptamers indicated that NOTA modification of aptamers and radiolabeling did not affect their secondary structures (SI Appendix, Fig. S17).

After successful synthesis of [^{68}Ga]Ga-NOTA-TRP-c, we first visualized the imaging probe in tumor-free Balb/c nude mice to evaluate the in vivo pharmacokinetics. PET/CT imaging was acquired at 30 min after intravenous administration of [^{68}Ga]Ga-NOTA-TRP-c (Fig. 3B). Because of its hydrophilic property and molecular weight, [^{68}Ga]Ga-NOTA-TRP-c was rapidly excreted through kidneys (8.71 ± 0.73%ID/g, $n = 3$) into the bladder (2.87 ± 0.74%ID/g, $n = 3$), along with enrichment in the liver (4.71 ± 0.52%ID/g, $n = 3$). A small amount of uptake was also found in the heart (0.44 ± 0.12%ID/g, $n = 3$), lung (0.46 ± 0.11%ID/g, $n = 3$) and muscle (0.20 ± 0.01%ID/g, $n = 3$) (Fig. 3C). The biological distribution analysis at 30 and 60 min post-injection also showed that accumulation in the kidney was higher [9.82 ± 0.20%ID/g (30 min); 6.5 ± 0.73 (60 min), $n = 3$], followed by liver [(7.57 ± 0.34%ID/g, 30 min; 6.54 ± 0.81%ID/g, 60 min, $n = 3$)] and bladder [(5.92 ± 0.18%ID/g, 30 min; 3.56 ± 0.82%ID/g, 60 min, $n = 3$)], further revealing the pharmacokinetics of [^{68}Ga]Ga-NOTA-TRP-c in tumor-free mice (Fig. 3D).

[^{68}Ga]Ga-NOTA-TRP-c PET imaging in subcutaneous SCLC models

Targeted tumor molecular imaging with [^{68}Ga]Ga-NOTA-TRP-c was studied in vivo, using subcutaneous RP-A21Lym- and SBC-2-bearing Balb/c nude mice, respectively. As shown in Fig. 4A and C, and SI Appendix, Fig. S18A, static imaging of 30 min and 60 min was acquired in RP-A21Lym mice after intravenous injection of [^{68}Ga]Ga-NOTA-TRP-c. Regions of interest (ROI) analysis (Fig. 4B and SI Appendix, Fig.

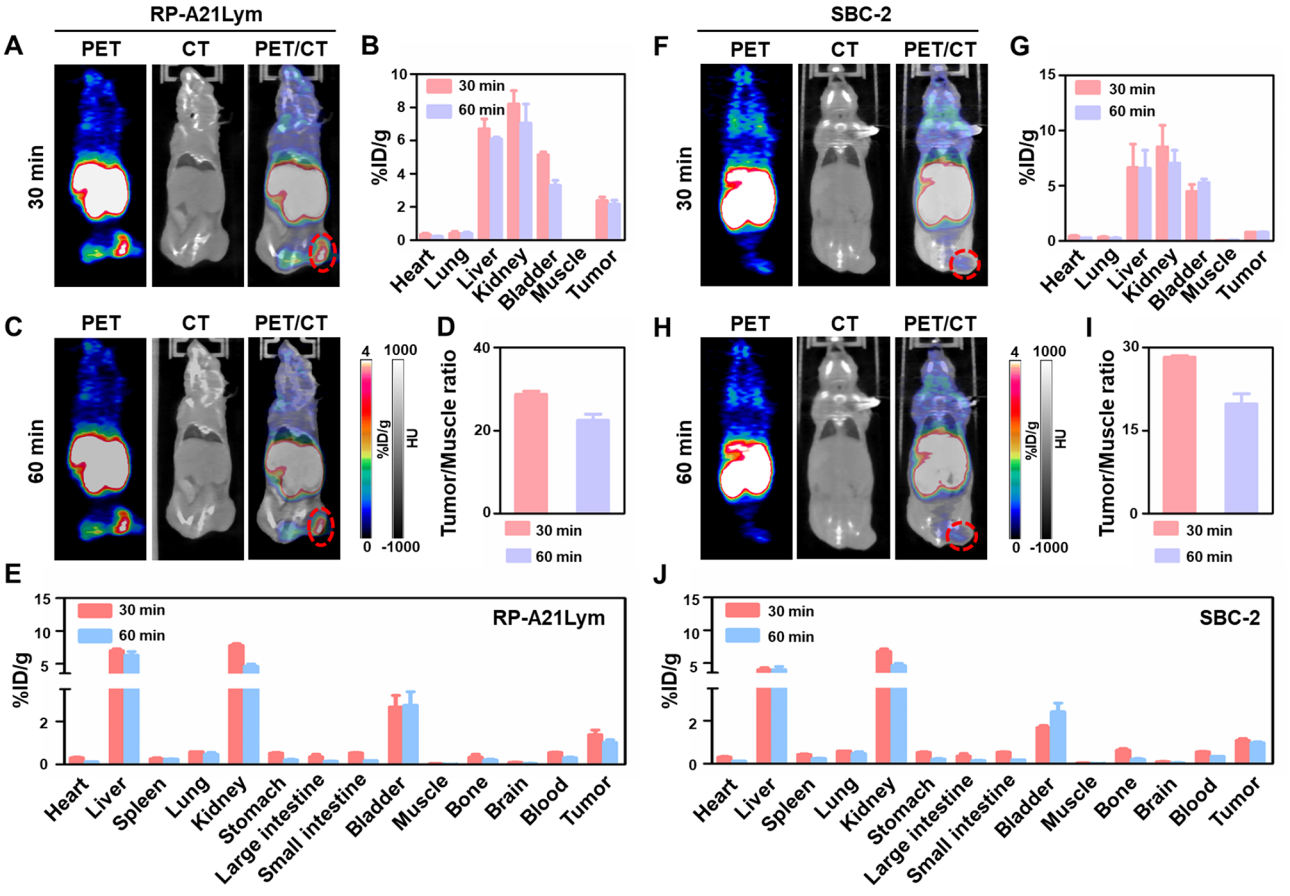

Fig. 4 [^{68}Ga]Ga-NOTA-TRP-c aptamer PET/CT imaging in SCLC tumor-bearing mice. Representative PET/CT imaging of [^{68}Ga]Ga-NOTA-TRP-c in RP-A21Lym-bearing Balb/c nude mice at 30 min (**A**) and 60 min (**C**) after intravenous administration. Tumor regions were labeled with red circles. (**B**) ROI data of [^{68}Ga]Ga-NOTA-TRP-c PET imaging analyzed from data in (**A**, **C**). (**D**) Ratio of [^{68}Ga]Ga-NOTA-TRP-c uptake by tumor versus muscle in RP-A21Lym-bearing Balb/c nude mice 30 min and 60 min after injection. (**E**) Biodistribution results of [^{68}Ga]Ga-NOTA-TRP-c in RP-A21Lym-bearing Balb/c nude mice after 30 min ($n = 3$) and 60 min ($n = 3$). Representative PET/CT imaging of [^{68}Ga]Ga-NOTA-TRP-c in human SCLC tumor cells by SBC-2-bearing Balb/c nude mice 30 min (**F**) and 60 min (**H**) after intravenous injection. Tumor regions were labeled with red circles. (**G**) ROI data of [^{68}Ga]Ga-NOTA-TRP-c PET imaging in SBC-2 mice analyzed from data in (**F**, **H**). (**I**) Ratio of [^{68}Ga]Ga-NOTA-TRP-c uptake by tumor versus muscle in SBC-2 mice at 30 min and 60 min after injection. (**J**) Biodistribution data in SBC-2 xenografts after injection of [^{68}Ga]Ga-NOTA-TRP-c at both 30 min ($n = 3$) and 60 min ($n = 3$)

S18B) showed that both groups possessed high kidney (8.23 ± 0.80%ID/g, $n = 3$), liver (6.71 ± 0.62%ID/g, $n = 3$), and bladder (5.15 ± 1.56%ID/g, $n = 3$) retention with a relatively clean background in other organs, consistent with the results of normal mice 30 min post-injection. Specific accumulation of [^{68}Ga]Ga-NOTA-TRP-c at tumor sites (1.52 ± 0.56%ID/g, $n = 3$) was clearly observed. The radioactivity of [^{68}Ga]Ga-NOTA-TRP-c in tumor was obviously higher than in muscle (Fig. 4D). Respective biological distribution results at 30 and 60 min post-injection further confirmed the targeted accumulation of [^{68}Ga]Ga-NOTA-TRP-c in RP-A21Lym tumor [1.39 ± 0.37%ID/g (30 min); 1.02 ± 0.22%ID/g (60 min), $n = 3$] (Fig. 4E). The imaging and biodistribution data in SBC-2-bearing nude mice are consistent with those in RP-A21Lym-bearing nude mice (Fig. 4F and H, and SI Appendix, Fig. S19A). ROI quantitative analysis results showed that the highest enrichment of [^{68}Ga]Ga-NOTA-TRP-c was found in the kidneys at 8.52 ± 1.96%ID/g after 30 min of injection and 6.64 ± 2.14%ID/g after 60 min of injection, followed by the liver at 7.05 ± 1.15%ID/g (30 min) and 6.59 ± 1.61%ID/g (60 min). The tumor uptake value was 0.80 ± 0.01%ID/g at 30 min and 0.80 ± 0.05%ID/g at 60 min post- injection ($n = 3$, Fig. 4G and SI Appendix, Fig. S19B). The enrichment ratio of [^{68}Ga]Ga-NOTA-TRP-c in tumor and muscle is more than 25 (Fig. 4I). The subsequent biodistribution analysis data presented the same trend of organ uptake as the ROI results with the highest kidney accumulation value of 6.76 ± 0.64%ID/g (30 min), followed by liver uptake of 3.97 ± 0.51%ID/g (30 min) and tumor uptake of 1.08 ± 1.05%ID/g (30 min) ($n = 3$, Fig. 4J). Meanwhile, [^{68}Ga]Ga-NOTA-TRP-c PET/CT imaging was also performed on a subcutaneous tumor-bearing mouse model of DMS 53 cells with moderate expression of Trop-2. The tumor uptake value was 1.06 ± 0.31%ID/g at 30 min and 0.75 ± 0.16%ID/g at 60 min post- injection ($n = 3$, SI Appendix, Fig. S20). Then, to evaluate screening capability and the ability to distinguish between Trop-2-positive and -negative tumors by [^{68}Ga]Ga-NOTA-TRP-c PET imaging, subcutaneous H446-bearing Balb/c nude mice were used as negative control. As expected, the static imaging and ROI results showed no tumor uptake post-intravenous administration of [^{68}Ga]Ga-NOTA-TRP-c in H446-bearing mice (SI Appendix, Fig. S21). In summary, [^{68}Ga]Ga-NOTA-TRP-c exhibited a high capacity for noninvasive assessment of Trop-2 positive expression in preclinical models of SCLC.

Therapeutic effect of SG on Trop-2-positive SCLC cells in vitro

To verify the possibility of using anti-Trop-2 aptamer-based molecular imaging for guiding SCLC targeted therapy, we evaluated the antitumor efficacy of anti-Trop-2 ADC on SCLC cells. As displayed in Fig. 5A and B, the apoptosis rate of SBC-2 cells increased significantly after SG treatment for 48 h, and the percentage of apoptotic cells rose with increasing drug concentration. In

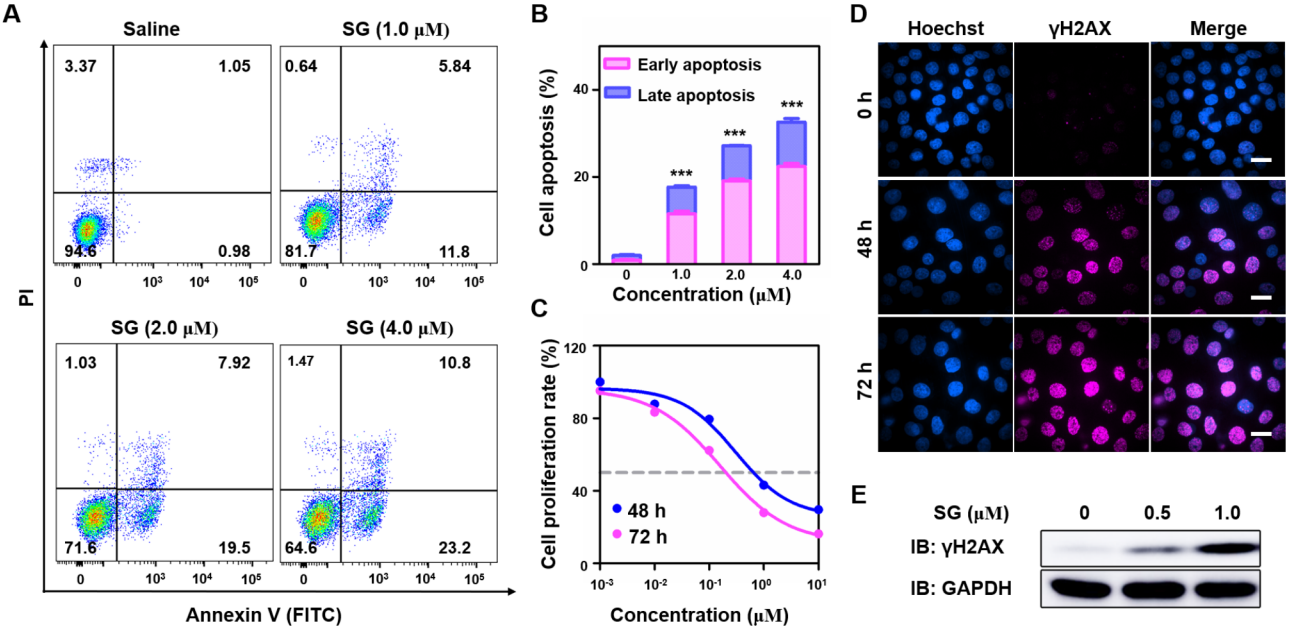

Fig. 5 Antitumor effect of anti-Trop-2 antibody-drug conjugate sacituzumab govitecan (SG) in SCLC tumor cells. (A) Cell apoptosis assay of SBC-2 cells after 48 h of treatment with different doses of SG (0, 1.0, 2.0, and 4.0 μM). (B) Quantitative determination of early and late apoptosis rates of SBC-2 cells treated with SG according to (A) results. *** Represents static significance versus saline group (0 μM) $p < 0.001$. (C) Cell proliferation curve of SBC-2 cells after 48 h and 72 h of treatment with gradient concentration of SG. (D) Representative images of DNA damage by γH2AX marker according to immunofluorescence in SBC-2 cells 48 h after 1.0 μm SG treatment. Scale bar, 20 μm. (E) Western blotting analysis of γH2AX in SBC-2 cells treated with SG

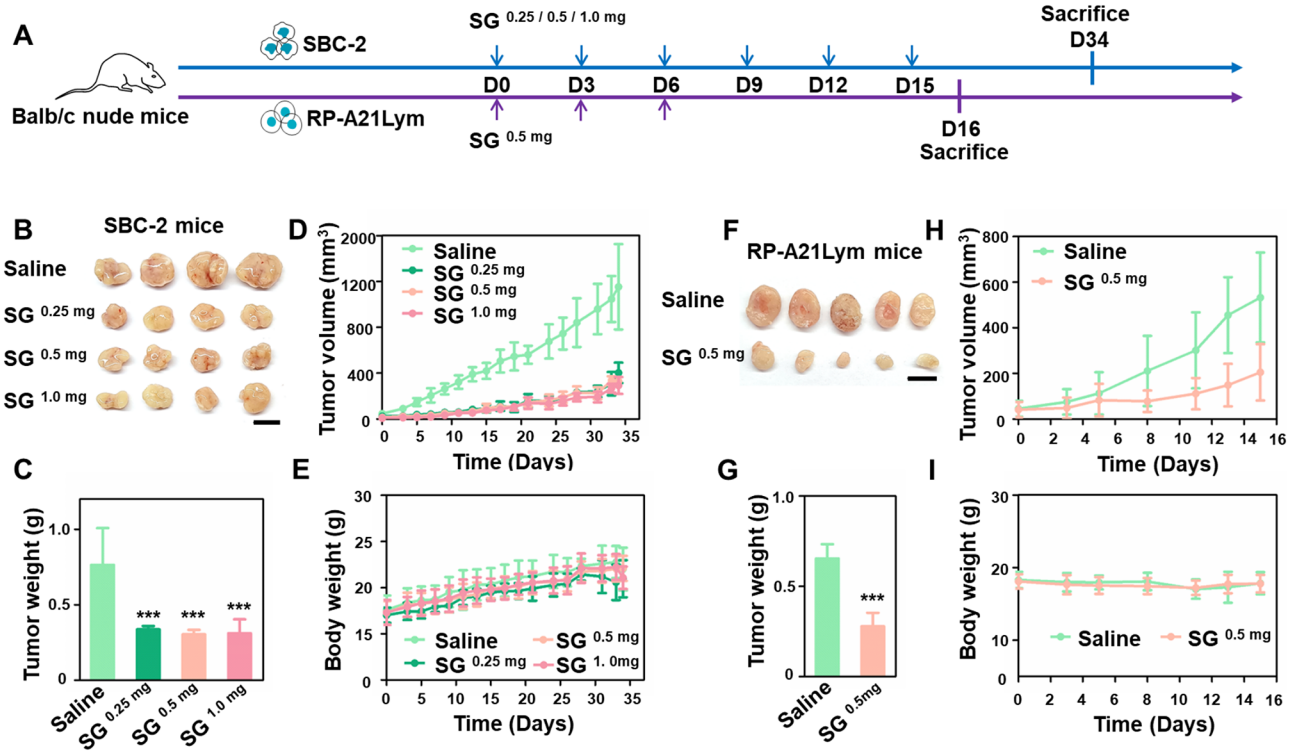

Fig. 6 Antitumor effect of anti-Trop-2 antibody-drug conjugate sacituzumab govitecan (SG) in vivo. (**A**) Schematic diagram of SG administration program for SBC-2 tumor- and primary mouse SCLC RP-A21Lym tumor-bearing nude mice. (**B**) Dissected tumors from SBC-2-bearing mice at day 34 after different dose of SG (0.25 mg, 0,5 mg, and 1.0 mg). Scale bar, 1.0 cm. (**C**) Tumor weights of SBC-2-bearing mice at the cutoff date. (**D**) Tumor growth curves for mice ($n = 4$/group) bearing SBC-2 cells treated with saline or SG (0.25 mg, 0.5 mg, and 1.0 mg). (**E**) Body weights of SBC-2-bearing mice treated by saline and SG. (**F**) Dissected tumor tissues from RP-A21Lym-bearing mice at day 16 after 0.5 mg SG. Scale bar, 1.0 cm. (**G**) Tumor weights from RP-A21Lym-bearing mice at day 16 after treatment with SG. (**H**) Relative tumor growth curves of RP-A21Lym-bearing mice after intravenous injection of SG. (**I**) Body weights of RP-A21Lym-bearing mice treated with SG

the 48 h and 72 h cell viability assays, SBC-2 cells were sensitive to SG with a decrease in cell proliferation rate; IC50 was 0.3068 μM (95% CI, 0.2224–0.4232 μM) and 0.1584 μM (95% CI, 0.1342–0.1868 μM), respectively (Fig. 5C). In addition, clonogenic assay showed an obvious decrease in the number of clones in the SG treatment group (SI Appendix, Fig. S22A and B). Consistent with SBC-2 results, SG also showed antitumor effects on RP-A21Lym according to the cell viability assay (SI Appendix, Fig. S23). In addition to these two Trop-2-positive cell lines which can be detected by [^{68}Ga]Ga-NOTA-TRP-c, we further verified the antitumor efficiency of SG on another Trop-2- overexpressing cell line, DMS 53, in vitro. The data demonstrated that SG had both short-term and long-term antitumor efficacy on DMS 53 cells, as revealed by CCK-8 and colony-forming assay (SI Appendix, Fig. S24). To further confirm the effect of SG on DNA damage resulting from antitumor effect on SCLC, we checked the expression of γH2AX, a molecular marker of DNA damage, using immunoblotting and IF assays. Compared to the saline group, the level of γH2AX was significantly elevated in SBC-2 and DMS-53 cells treated with SG (Fig. 5D and E, and SI Appendix, Fig. S25). Thus, these data suggest that SG exhibited excellent antitumor effect on SCLC cells with positive expression of Trop-2.

Antitumor efficiency of SG in SCLC tumors with [^{68}Ga]Ga-NOTA-TRP-c accumulation

Based on the results of antitumor efficiency in vitro, we carried out an in vivo investigation in SCLC subcutaneous xenografts with a high level of Trop-2 expression successfully screened by [^{68}Ga]Ga-NOTA-TRP-c. The treatment strategies for different tumor models were illustrated in Fig. 6A. First, in order to determine the appropriate dose for efficacy studies in SCLC, SBC-2-bearing mice were divided into four groups, representing different SG dosage (0 mg, 0.25 mg, 0.5 mg and 1.0 mg per mouse per time). The tumor-bearing mice were treated on day 0, 3, 6, 9, 12 and 15, respectively. After mice were sacrificed on day 34, the weight and size of each tumor were recorded by dissecting the tumor ex vivo. Compared with the control group, all dose groups of SG induced stasis and tumor regression without weight loss (Fig. 6B-E, and SI Appendix, Fig. S26). After treatments, the assessment of serum levels of white blood

cells (WBC), red blood cells (RBC), and blood platelets (PLT) was conducted as the indicator of hematological toxicity, and SG showed no hematological toxicity (SI Appendix, Fig. S27). In addition, pathological analysis of the heart, liver, spleen, lung, and kidney demonstrated no obvious histological changes after all SG treatments compared with the saline group (SI Appendix, Fig. S28). Additionally, the serum levels of aspartate aminotransferase (AST), alanine aminotransferase (ALT), and direct bilirubin (DBIL) were tested as the indicators of hepatic function of the mice. As shown in SI Appendix, Fig. S29, 1 mg SG injection showed slight increase in DBIL level with a significant p-value, which demonstrated the safety of using a relatively low dose of SG (0.25 mg and 0.5 mg) during SCLC treatment in Balb/c nude mice. Next, we further evaluated the effectiveness of SG in RP-A21Lym-bearing mice, and 0.5 mg SG per mouse per time were used as the treatment formulation. Mice treated with SG also showed high inhibition in tumor growth without weight loss (Fig. 6F-I, and SI Appendix, Fig. S30). For tumors models that were not recognized by [^{68}Ga]Ga-NOTA-TRP-c, we evaluated whether SG had a therapeutic effect. H446 subcutaneous tumor-bearing mice were divided into two groups, control group and SG treatment group, as shown in SI Appendix, Fig. S31, there were no statistical differences in tumor growth between the control group and the SG treatment group. In order to initially explore the mechanism of effect caused by SG, the immunoblotting analysis from subcutaneous tumor tissues showed that SG inhibited tumor growth by causing DNA damage in SCLC (SI Appendix, Fig. S32), which is consistent with the results of in vitro experiments. Finally, we explored whether cell membrane Trop-2 antigen expression level could be decreased during SG therapy, leading, in turn, to concerns over treatment deficiencies and lack of visualization in vivo using [^{68}Ga]Ga-NOTA-TRP-c PET imaging. Western blotting analysis showed that SG neither significantly affected the overall protein expression level of Trop-2 in SBC-2 cells (SI Appendix, Fig. S33A and B) nor in tumor tissues of SBC-2-bearing mice (SI Appendix, Fig. S33C and D). Representative immunohistochemical images of subcutaneous tumor tissues further showed no difference in the expression of Trop-2 between the control group and the SG group (SI Appendix, Fig. S34). More important, to annotate the role of anti-Trop-2 aptamer in detecting Trop-2 during SG treatment in SCLC, we conducted [^{68}Ga]Ga-NOTA-TRP-c PET imaging before and after SG treatment, and the results showed that noninvasive PET imaging using [^{68}Ga]Ga-NOTA-TRP-c could visualize no changes in Trop-2 tumoral expression during SG treatment as long as the SCLC xenograft tumors existed (SI Appendix, Fig. S35A, B, and C). Overall, SG treatment was efficient in Trop-2-positive SCLC tumors, and Trop-2 expression could be monitored before and after therapy with anti-Trop-2 aptamer.

Discussion

Besides NSCLC, a considerable number of patients with SCLC showed high expression of Trop-2, thus, anti-Trop-2 ADC may be a therapeutic option. However, since less than 1% of patients with SCLC have surgical tissue specimens, most patients must undergo bronchoscopic biopsy. This places a limitation on tumor samples, along with the correspondingly high chance of getting necrotic pathological tissues, thus posing a challenge to the comprehensive assessment of Trop-2 expression level and making clinical therapeutic response unpredictable for SCLC patients. So far, antibody-based targeting probes for Trop-2 PET imaging have been studied in preclinical prostate and pancreatic models, and the results demonstrated the possibility and potential of Trop-2-based molecular imaging in solid tumors. However, the high molecular weight conferred many shortcomings on antibody probes, such as complex production, long clearance half-life, and long interval between injection and PET imaging, making it difficult to obtain acceptable images. As we highlighted above, aptamers are single-stranded nucleic acids with specific binding function, and they possess such merits as simple synthesis and radiolabeling, excellent thermal stability, and rapid clearance. Recent approaches have demonstrated the feasibility and safety of utilizing aptamer-based molecular imaging in the clinical setting, and numerous preclinical studies highlighted the efficacy of aptamer-based imaging probes in various common solid tumors. Therefore, we rationally designed and fabricated an anti-Trop-2 aptamer PET imaging probe and studied whether the expression of Trop-2 in SCLC could be specifically assessed by aptamer-based molecular imaging. Indeed, our studies did show that this anti-Trop-2 aptamer probe was able to potentially guide the use of Trop-2 targeted therapy in preclinical SCLC models.

As one of the latest FDA approved ADCs, anit-Trop-2 sacituzumab govitecan has demonstrated its antitumor efficacy in most epithelial cancers. It has achieved success and is considered as a major breakthrough in triple-negative breast cancer management, leading to the increasing number of clinical trials being conducted to validate the efficacy of SG as an anti-Trop-2 ADC in various solid tumors. While several SCLC cohorts are ongoing with variable results among them, it is clear that accurate and thorough evaluation of Trop-2 expression in patients is critical to achieving a good ORR. To the best of our knowledge, only a few antibody-based immunoPET probes were developed for noninvasive Trop-2 expression evaluation, and no studies have, so far, reported on aptamers targeting Trop-2 in lung cancer. More

importantly, the association between Trop-2 expression levels, as evaluated by molecular imaging, and subsequent therapeutic effectiveness of anti-Trop-2-targeted therapy was rarely studied. This begs the question of whether aptamer-based PET imaging can be used to detect Trop-2 expression and, hence, aid in the identification of SCLC patients who would benefit from anti-Trop-2 ADC therapy. In pursuit of addressing this question, we first evaluated the expression of Trop-2 expression in SCLC tumor samples from clinical patients and several SCLC cell lines, and the results revealed heterogeneous expression of Trop-2 in SCLC, which emphasized the importance of developing novel noninvasive detection methods to screen Trop-2-positive tumors in SCLC patients. Next, we designed and optimized a single-stranded anti-Trop-2 DNA aptamer containing 46 oligonucleotides TRP-c with excellent specificity. The specific targeting ability of TRP-c was then demonstrated not only in Trop-2-overexpressing SCLC cells, but also in the respective SCLC tumor animal models. After an elaborate radiolabeling process, we performed PET/CT imaging with [^{68}Ga]Ga-NOTA-TRP-c in human and mouse SCLC models. In essence, aptamers are recognition elements with homing properties enabling them to, in this case, specifically bind to Trop-2 antigens, regardless of whether they are overexpressed in murine- or human-derived models. Since [^{68}Ga]Ga-NOTA-TRP-c did not react with Trop-2-negative H446-bearing mice, this aptamer-based PET imaging probe demonstrated the ability to differentiate positive and negative expression of Trop-2 in preclinical models. In addition, compared to several previously reported aptamer-based radionuclide imaging probes, such as AS1411 [23], SGC8 [21] and MinE07 [24], the tumor-to-muscle ratio of [^{68}Ga]Ga-NOTA-TRP-c is much higher (25 for TRP-c, 2 for AS1411, 10.25 for SGC8, and 8.65 for MinE07), demonstrating its superiority in PET imaging. Taking advantage of the radiolabeled anti-Trop-2 aptamer in detecting Trop-2-positive tumors, it was considered plausible to evaluate the therapeutic efficacy of anti-Trop-2 ADC in [^{68}Ga]Ga-NOTA-TRP-c screened tumors, which has not been studied in preclinical SCLC. We found that SG showed significant antitumor effect in SCLC mouse models with adequate uptake of radiolabeled anti-Trop-2 aptamer, which suggested that anti-Trop-2 aptamer-based PET might be a critical addition to the toolkit for the management of SCLC patients for whom SC treatment might be a viable option.

There are several inherent limitations in this study. First, this study focuses on the development of nucleic acid aptamer-based probes specifically targeting Trop-2 for application in SCLC screening. However, this aptamer does not involve any chemical modifications. Although the TRP-c aptamer satisfies the imaging requirements, it is still susceptible to enzymatic cleavage over long periods of in vivo use. Further chemical modifications are urgently needed to improve the pharmacokinetics of the aptamer and enable long-half-life radionuclide labeling, which would allow for long-term monitoring of Trop-2 expression during therapy. Second, the potential for TRP-c aptamer-guided radionuclide therapy has not been explored. While the targeted imaging capability of the TRP-c aptamer has been confirmed in this study, future work will investigate the theranostic pair of ^{68}Ga and ^{177}Lu to achieve intravenous imaging of Trop-2 expression in SCLC patients, along with respective targeted radionuclide therapy.

Conclusion

In summary, we evaluated Trop-2 expression levels, both in SCLC clinical samples and cell lines, and verified the heterogeneous expression of Trop-2 across SCLC. By presenting an initial report of anti-Trop-2 aptamer-based molecular imaging in SCLC, we revealed an anti-Trop-2 aptamer as a functional oligonucleotide in detecting Trop-2 expression in vitro and in vivo. Furthermore, owing to the special properties of aptamers, this anti-Trop-2 aptamer was successfully radiolabeled to fabricate a molecular imaging probe, [^{68}Ga]Ga-NOTA-TRP-c. This novel targeted imaging probe achieved identification of Trop-2-positive tumors, either in murine- or human-derived tumor animal models. Further investigation proved that this imaging probe accurately evaluated Trop-2-overexpressing cell lines and that tumor models responded well after receiving SG treatment, demonstrating that in situ evaluation of Trop-2 expression could be an integral part of the clinician's diagnostic toolkit to identify personalized treatment strategies and precisely evaluate therapeutic outcomes in SCLC.

Materials and methods

Cell lines

Human SCLC cell lines SBC-2 and H446 were purchased from WheLab (Shanghai, China), DMS 53 and SW1271 were purchased from MeisenCTCC (Meisen Chinese Tissue Culture Collections). Primary murine SCLC cell line RP-A21Lym derived from the genetically engineered mouse model was kindly provided by Professor Hongbin Ji (CAS Center for Excellence in Molecular Cell Science, Chinese Academy of Sciences). Human SCLC cell lines were maintained in RPMI medium 1640 (Gibco) supplemented with 10% FBS (Cytiva, Massachusetts, USA) and 1% penicillin/streptomycin (Sangon Biotech, Shanghai, China), and RP-A2Lym cells were cultured in the same complete RPMI medium 1640 supplemented with Insulin-Transferrin (Gibco) and β-estradiol (Sigma). All cell lines were authenticated through short-tandem repeat profiling and confirmed to be mycoplasma-negative.

Mouse models

Animal care and experimental procedures were performed in accordance with the guidelines of the Institutional Animal Care and Use Committee (Renji Hospital, School of Medicine, Shanghai Jiao Tong University). All experimental procedures related to animals were approved by the Animal Care and Use Committee of Renji Hospital. Six-week-old female BALB/c-nude mice were purchased from Hangzhou Ziyuan Experimental Animal Technology Co., Ltd.

Human tissue specimens

In this study, a total of 53 Human paraffin embedded SCLC tissue samples were retrospectively collected from Zhejiang Cancer Hospital, which in accordance with the Institutional Review Board/Privacy Board at the Zhejiang Cancer Hospital for retrospective review of records and waiver of consent.

Immunohistochemistry and hematoxylin-eosin staining

Human SCLC tissue samples, normal tissues and tumors from SCLC-bearing mice were fixed overnight in 4% paraformaldehyde (Sangon Biotech, Shanghai, China). Then, they were dehydrated and embedded. Serial sections with a thickness of 4 μm from all human and murine formalin-fixed paraffin-embedded samples were cut onto glass slides, followed by staining with anti-Trop-2 antibodies (1:200) according to the manufacturer's protocol. All hematoxylin-eosin (HE) and Immunohistochemistry (IHC) staining images were captured under a digital pathology slide scanner (KFBIO, Soochow, China). Primary antibodies against Trop-2 (EPR20044) were purchased from Abcam.

Quantitative real-time PCR

Total RNA was extracted using TRIzol reagent (Takara). Reverse transcription of total RNA was performed using PrimeScript™ RT master reagent kit (Takara). Quantitative real-time PCR was carried out using SYBR Mixture (Takara) and Roche Cobas Z 480 Real Time PCR system. Ct value of GAPDH was used for relative quantification. The relative mRNA levels of Trop-2 were calculated using the $2^{-\Delta\Delta Ct}$ method.

Primers of Trop-2:
Forward: 5'-GCCTACTACTTCGAGAGGGACA-3'
Reverse: 5'-CAGTTCCTTGATCTCCACCTTC-3'
Primers of GAPDH:
Forward: 5'-TGACTTCAACAGCGACACCCA-3'
Reverse: 5'-CACCCTGTTGCTGTAGCCAAA-3'

In vitro cell targeting and cellular uptake of aptamers

To visually evaluate SCLC cells that bind with aptamers, each cell line (4×10^5 cells) was cultured on a glass-bottomed dish for 24 h. Next, cells were washed with washing buffer (Dulbecco's phosphate-buffered saline (DPBS) supplemented with 4.5 mg/mL glucose and 5 mM $MgCl_2$) twice and then incubated with DNA aptamers (250 nM) in binding buffer (washing buffer supplemented with 0.1 mg/mL tRNA and 1 mg/mL BSA) at 4 °C for 30 min. To test aptamer endocytosis, cells were incubated with aptamer in culture medium at 37 °C for 3 h in a carbon dioxide incubator. After washing three times with washing buffer, all samples were visualized with a Nikon CSU-W1 SoRa microscope. To test for cell binding using flow cytometry, cells (5×10^5 cells) were washed with washing buffer at 4 °C and then incubated with aptamers in binding buffer at 4 °C for 30 min. After washing three times with washing buffer at 4 °C, samples were analyzed via a BD FACSVerse™ system.

Immunoblotting and immunofluorescence (IF) assay

For western blotting, whole-cell extracts were obtained from cell lines or tumor tissues. Twenty micrograms of whole proteins were mixed with loading buffer and boiled at 100 °C for 10 min. 10% SDS-PAGE gels (constant pressure 100 V, 80 min) were used to separate the proteins. Proteins were transferred to the PVDF membrane (Millipore) and further incubated with appropriate antibodies. Immobilon Western Chemiluminescent HRP Substrate (Millipore) was used for protein detection. Relative protein levels were quantified by Image J software. For immunofluorescence, 4×10^5 cells were cultured on a glass-bottomed dish for 24 h. After three washes using DPBS, cells were fixed with 4% paraformaldehyde for 20 min, permeabilized using Triton X-100 (Beyotime Biotechnology) for 15 min, and then stained with specific antibodies. Representative images were captured by a Nikon CSU-W1 SoRa system or Zeiss TCS SP8 confocal microscope. Primary and secondary antibodies used were as follows: anti-Trop-2 (EPR20044, Abcam), anti-γH2AX (CST), anti-GAPDH (Sigma), HRP-Rabbit-anti-human (Sigma), and HRP-mouse-anti-human (Abcam).

Conjugation and radiolabeling of anti-Trop-2 aptamer

Aptamers used for flow cytometry were labeled with a Cy5 dye at the 5′-end, and all sequences were synthesized by Sangon Biotech (Shanghai, China). NOTA-anti-Trop-2 aptamer was synthesized by conjugation of NOTA-NHS with 5′ amino-modified anti-Trop-2 aptamer, which was produced by Biosyntech (Soochow, China). NH_2-TRP-c was dissolved in 0.1 M sodium bicarbonate, and NOTA-NHS was dissolved in DMSO. The NOTA solution and NH_2-TRP-c solution were mixed and incubated on a constant-temperature shaker at room temperature for 120 min. The molecular weights of all final products were confirmed by mass spectrum, and the purity was tested by HPLC. For radiolabeling, NOTA-anti-Trop-2 aptamer (3 nmol) was dissolved in sodium acetate aqueous buffer

(1 M, 156 μl) and mixed with $^{68}GaCl_3$ solution (1 ml) acquired from the $^{68}Ge/^{68}Ga$ generator (IGG100, Eckert & Ziegler) with 0.1 M HCl elution. Next, the solution was reacted for 20 min at 100 °C in a metal incubator and then cooled down to room temperature (RT) afterward. Then, the mixture was passed through a PD-10 column (GE Healthcare) to obtain purified [^{68}Ga]Ga-NOTA-anti-Trop-2 aptamer. Instant thin-layer chromatography (iTLC) and HPLC were used to measure the radiochemical purity and stability of [^{68}Ga]Ga-NOTA-anti-Trop-2 aptamer. The radioactive labeling efficiency and purity of the final product was determined by iTLC (0.25 M sodium citrate as the mobile phase) (Eckert & Ziegler Radiopharma, Inc.) and HPLC equipped with a radioactive detector (Agilent).

In vivo fluorescence imaging

The cell suspensions (5×10^6 cells per mouse, treated in DPBS with Matrigel (Corning) at 1:1 (v/v)) were subcutaneously inoculated into the right hind limb or armpit of mice. After 3–4 weeks, whole body imaging was performed 30 min after intravenous injection of aptamer strands with 1 nmol using the IVIS in vivo imaging system (IVIS® Lumina Series III, PerkinElmer, USA). Then, heart, liver, spleen, lung, kidney, and tumor were harvested to estimate organ distribution of oligonucleotides. The quantification of absolute fluorescence intensity after background subtraction was calculated for each organ and tumor using the IVIS software. Statistical analysis was performed using GraphPad Prism 5.0 (GraphPad Software, Boston, USA). There was significant difference in 95% confidence interval when p value ≤ 0.05.

Micro PET/CT imaging and ex vivo biodistribution analysis

The radiolabeled aptamer [^{68}Ga]Ga-NOTA-TRP-c used for in vivo studies had a radiochemical purity over 95% and molar activity in the range of 11.1–16.5 MBq/nmol. Briefly, mice were intravenously injected with 3.7–7.4 MBq of [^{68}Ga]Ga-NOTA-TRP-c, anesthetized with 2% isoflurane, and then positioned on the scanning bed. In vivo PET/CT imaging of mice was obtained using the Inveon small-animal PET scanner (Siemens Healthineers, Germany). PET/CT imaging was acquired at 30 min and 60 min post-injection. Inveon Research Workplace 4.2 was used to analyze the ROI data presented as the percentage of injected dose per gram of tissue (%ID/g). For ex vivo biodistribution experiments, mice were injected with 3.7 MBq of [^{68}Ga]Ga-NOTA-TRP-c ($n = 3$ per group). At 30 min and 60 min post-injection, mice were sacrificed and dissected. Major normal organs, blood and tumors were collected and weighed. Radioactivity was measured by using a γ-counter (SN-6110, Rihuan Optoelectronic Instruments, Shanghai, China). The results were presented as %ID/g.

Detection of cell proliferation and cell apoptosis

For cell proliferation, 1×10^4 cells were cultured in wells of a 96-well plate and allowed to attach overnight before exposure to SG. After 48 h or 72 h of treatment, new medium containing 10% cell counting kit 8 (CCK-8, Beyotime Biotechnology) was added to the plates. Absorbance was measured at 450 nm after 1–2 h of incubation in a carbon dioxide incubator. Normalized transformed dose-response curves were analyzed using GraphPad Prism. For cell apoptosis, 5×10^5 cells were cultured in wells of a 6-well plate overnight and collected using 0.25% trypsin solution without EDTA 48 h after saline or SG treatment. Subsequently, cells were stained with Annexin V-FITC for 10 min and PI for 5 min at RT using the Annexin-V-FITC/PI apoptosis kit (Vazyme, Nanjing, China) according to the manufacturer's instructions. Stained cells were analyzed via the BD FACSVerse™ system.

Therapeutic studies using SCLC tumor xenografts

Five million SBC-2, H446 and RP-A21Lym cells were subcutaneously injected into Balb/c nude mice. Tumor volume (mm^3) was calculated as Length × $Width^2 \times 0.5$. After tumor size reached approximately 50 mm^3, mice were randomly assigned to each group. The treatment was started through intravenous injection of saline or SG administered once every three days. In SBC-2-bearing mice, the doses of SG were designed as 0.25 mg, 0.5 mg and 1.0 mg per mouse per time to explore the appropriate dosage using preclinical SCLC mode, and according to this result, a dose of 0.5 mg SG was administered to H446 and RP-A21Lym-bearing mice per time. Tumor dimensions were obtained every 2 or 3 days with a caliper. Mice were euthanized, and tumors and normal tissues were isolated until mice reached a set endpoint (severe petechiae, more than 20% weight loss, tumor volume ≥ 1,800 mm^3, or the tumors developed ulceration). Samples were snap-frozen in liquid nitrogen for protein isolation or fixed in 4% paraformaldehyde and processed for paraffin histologic analysis. Sections of paraffin-embedded tissues (4 μm) were stained with H&E or IHC.

Quantification and statistical analysis

The data obtained in this study were processed and analyzed by GraphPad Prism. Student's t-test was used to compare the difference between two groups, while one-way analysis of variance (ANOVA) was used to compare the difference between more than two groups. P value ≤ 0.05 was regarded as statistical significance.

Supplementary Information

The online version contains supplementary material available at https://doi.org/10.1186/s12951-025-03184-6 .

Supplementary Material 1

Acknowledgements
D.D. acknowledges the Shanghai Sailing Program, Shanghai Committee of Science and Technology, China (No. 21YF1425700), and Innovative research team of high-level local universities in Shanghai, China.

Author contributions
D.D., S.S. and W.T. contributed to project conception, organization and execution. Y.C., X.L. and K.L. conducted experiments, collected and analyzed data, and contributed to the preparation and writing of the manuscript. Y.S. was responsible for aptamer sequence truncate and optimization. Y.C. wrote the first draft of the manuscript. D.D., and W.T. reviewed and edited the final draft of the manuscript.

Funding
This work was supported by the National Key Research and Development Program of China (No. 2020YFA0909000), Fundamental Research Funds for the Central Universities (2020JCPT02), and National Nature Science Foundation of China (No. 22204102, No. 91953000, No. 2182781).

Data availability
No datasets were generated or analysed during the current study.

Declarations

Ethics approval and consent to participate
Small cell lung cancer tumor samples were retrospectively conducted from Zhejiang Cancer Hospital, which in accordance with the Institutional Review Board/Privacy Board at the Zhejiang Cancer Hospital for retrospective review of records and waiver of consent. Animal experiments was approved by the Institutional Animal Care and Use Committee of Renji Hospital.

Competing interests
The authors declare no competing interests.

Author details
[1]Institute of Molecular Medicine (IMM), Shanghai Key Laboratory for Nucleic Acid Chemistry and Nanomedicine, Renji Hospital, Shanghai Jiao Tong University School of Medicine, Shanghai 200240, China
[2]Department of Nuclear Medicine, Fudan University Shanghai Cancer Center, Shanghai 200032, China
[3]The Cancer Hospital of the University of Chinese Academy of Sciences (Zhejiang Cancer Hospital), Hangzhou Institute of Medicine (HIM), Chinese Academy of Sciences, Hangzhou, Zhejiang 310022, China

Received: 29 October 2024 / Accepted: 1 February 2025
Published online: 06 March 2025

References

1. Siegel RL, Giaquinto AN, Jemal A. Cancer statistics, 2024. CA Cancer J Clin. 2024;74(1):12–49.
2. Rudin CM, Brambilla E, Faivre-Finn C, Sage J. Small-cell lung cancer. Nat Rev Dis Primers. 2021;7(1):3.
3. Inoue M, Sawabata N, Okumura M. Surgical intervention for small-cell lung cancer: what is the surgical role? Gen Thorac Cardiovasc Surg. 2012;60(7):401–5.
4. Sabari JK, Lok BH, Laird JH, Poirier JT, Rudin CM. Unravelling the biology of SCLC: implications for therapy. Nat Rev Clin Oncol. 2017;14(9):549–61.
5. Dingemans AC, Fruh M, Ardizzoni A, Besse B, Faivre-Finn C, Hendriks LE, Lantuejoul S, Peters S, Reguart N, Rudin CM, et al. Small-cell lung cancer: ESMO Clinical Practice guidelines for diagnosis, treatment and follow-up (☆). Ann Oncol. 2021;32(7):839–53.
6. Lee JH, Saxena A, Giaccone G. Advancements in small cell lung cancer. Semin Cancer Biol. 2023;93:123–8.
7. Megyesfalvi Z, Gay CM, Popper H, Pirker R, Ostoros G, Heeke S, Lang C, Hoetzenecker K, Schwendenwein A, Boettiger K, et al. Clinical insights into small cell lung cancer: Tumor heterogeneity, diagnosis, therapy, and future directions. CA Cancer J Clin. 2023;73(6):620–52.
8. Cubas R, Li M, Chen C, Yao Q. Trop2: a possible therapeutic target for late-stage epithelial carcinomas. Biochim Biophys Acta. 2009;1796(2):309–14.
9. Trerotola M, Cantanelli P, Guerra E, Tripaldi R, Aloisi AL, Bonasera V, Lattanzio R, de Lange R, Weidle UH, Piantelli M, et al. Upregulation of Trop-2 quantitatively stimulates human cancer growth. Oncogene. 2013;32(2):222–33.
10. Jiang A, Gao X, Zhang D, Zhang L, Lu H. Expression and clinical significance of the Trop-2 gene in advanced non-small cell lung carcinoma. Oncol Lett. 2013;6(2):375–80.
11. Mito R, Matsubara E, Komohara Y, Shinchi Y, Sato K, Yoshii D, Ohnishi K, Fujiwara Y, Tomita Y, Ikeda K, et al. Clinical impact of TROP2 in non-small lung cancers and its correlation with abnormal p53 nuclear accumulation. Pathol Int. 2020;70(5):287–94.
12. Guerra E, Trerotola M, Aloisi AL, Tripaldi R, Vacca G, La Sorda R, Lattanzio R, Piantelli M, Alberti S. The Trop-2 signalling network in cancer growth. Oncogene. 2013;32(12):1594–600.
13. Parisi C, Mahjoubi L, Gazzah A, Barlesi F. TROP-2 directed antibody-drug conjugates (ADCs): the revolution of smart drug delivery in advanced non-small cell lung cancer (NSCLC). Cancer Treat Rev. 2023;118:102572.
14. Gray JE, Heist RS, Starodub AN, Camidge DR, Kio EA, Masters GA, Purcell WT, Guarino MJ, Misleh J, Schneider CJ, et al. Therapy of small cell Lung Cancer (SCLC) with a Topoisomerase-I-inhibiting antibody-drug conjugate (ADC) targeting Trop-2, Sacituzumab Govitecan. Clin Cancer Res. 2017;23(19):5711–9.
15. Bardia A, Messersmith WA, Kio EA, Berlin JD, Vahdat L, Masters GA, Moroose R, Santin AD, Kalinsky K, Picozzi V, et al. Sacituzumab Govitecan, a trop-2-directed antibody-drug conjugate, for patients with epithelial cancer: final safety and efficacy results from the phase I/II IMMU-132-01 basket trial. Ann Oncol. 2021;32(6):746–56.
16. Bardia A, Tolaney SM, Punie K, Loirat D, Oliveira M, Kalinsky K, Zelnak A, Aftimos P, Dalenc F, Sardesai S, et al. Biomarker analyses in the phase III ASCENT study of sacituzumab govitecan versus chemotherapy in patients with metastatic triple-negative breast cancer. Ann Oncol. 2021;32(9):1148–56.
17. Marjani AA, Nader ND, Aghanejad A. Exosomes as targeted diagnostic biomarkers: recent studies and trends. Life Sci. 2024;354:122985.
18. Kheyrolahzadeh K, Tohidkia MR, Tarighatnia A, Shahabi P, Nader ND, Aghanejad A. Theranostic chimeric antigen receptor (CAR)-T cells: insight into recent trends and challenges in solid tumors. Life Sci. 2023;328:121917.
19. Tan W, Donovan MJ, Jiang J. Aptamers from cell-based selection for bioanalytical applications. Chem Rev. 2013;113(4):2842–62.
20. Dunn MR, Jimenez RM, Chaput JC. Analysis of aptamer discovery and technology. Nat Rev Chem. 2017;1(10).
21. Jacobson O, Weiss ID, Wang L, Wang Z, Yang X, Dewhurst A, Ma Y, Zhu G, Niu G, Kiesewetter DO, et al. 18F-Labeled single-stranded DNA aptamer for PET imaging of protein tyrosine Kinase-7 expression. J Nucl Med. 2015;56(11):1780–5.
22. Jacobson O, Yan X, Niu G, Weiss ID, Ma Y, Szajek LP, Shen B, Kiesewetter DO, Chen X. PET imaging of tenascin-C with a radiolabeled single-stranded DNA aptamer. J Nucl Med. 2015;56(4):616–21.
23. Park JY, Lee TS, Song IH, Cho YL, Chae JR, Yun M, Kang H, Lee JH, Lim JH, Cho WG, et al. Hybridization-based aptamer labeling using complementary oligonucleotide platform for PET and optical imaging. Biomaterials. 2016;100:143–51.
24. Cheng S, Jacobson O, Zhu G, Chen Z, Liang SH, Tian R, Yang Z, Niu G, Zhu X, Chen X. PET imaging of EGFR expression using an (18)F-labeled RNA aptamer. Eur J Nucl Med Mol Imaging. 2019;46(4):948–56.
25. Ding D, Zhao H, Wei D, Yang Q, Yang C, Wang R, Chen Y, Li L, An S, Xia Q, et al. The First-in-human whole-body dynamic pharmacokinetics study of Aptamer. Res (Wash D C). 2023;6:126.
26. van Rij CM, Sharkey RM, Goldenberg DM, Frielink C, Molkenboer JD, Franssen GM, van Weerden WM, Oyen WJ, Boerman OC. Imaging of prostate cancer with immuno-PET and immuno-SPECT using a radiolabeled anti-EGP-1 monoclonal antibody. J Nucl Med. 2011;52(10):1601–7.
27. van Rij CM, Lutje S, Frielink C, Sharkey RM, Goldenberg DM, Franssen GM, Mcbride WJ, Rossi EA, Oyen WJ, Boerman OC. Pretargeted immuno-PET and radioimmunotherapy of prostate cancer with an anti-TROP-2 x anti-HSG bispecific antibody. Eur J Nucl Med Mol Imaging. 2013;40(9):1377–83.
28. Chen W, Li M, Younis MH, Barnhart TE, Jiang D, Sun T, Lang JM, Engle JW, Zhou M, Cai W. ImmunoPET of trophoblast cell-surface antigen 2 (Trop-2) expression in pancreatic cancer. Eur J Nucl Med Mol Imaging. 2022;49(3):861–70.
29. Li C, Liu J, Yang X, Yang Q, Huang W, Zhang M, Zhou D, Wang R, Gong J, Miao Q, et al. Theranostic application of (64) Cu/ (177) Lu-labeled anti-Trop2

monoclonal antibody in pancreatic cancer tumor models. Eur J Nucl Med Mol Imaging. 2022;50(1):168–83.
30. Huang W, Liang C, Zhang Y, Zhang D, An S, Wu Q, Li J, Zhao H, Wang C, Cui J, et al. ImmunoPET imaging of Trop2 expression in solid tumors with nanobody tracers. Eur J Nucl Med Mol Imaging. 2024;51(2):380–94.
31. Qu S, Fetsch P, Thomas A, Pommier Y, Schrump DS, Miettinen MM, Chen H. Molecular subtypes of primary SCLC tumors and their associations with neuroendocrine and therapeutic markers. J Thorac Oncol. 2022;17(1):141–53.
32. Megyesfalvi Z, Barany N, Lantos A, Valko Z, Pipek O, Lang C, Schwendenwein A, Oberndorfer F, Paku S, Ferencz B, et al. Expression patterns and prognostic relevance of subtype-specific transcription factors in surgically resected small-cell lung cancer: an international multicenter study. J Pathol. 2022;257(5):674–86.
33. Baine MK, Febres-Aldana CA, Chang JC, Jungbluth AA, Sethi S, Antonescu CR, Travis WD, Hsieh MS, Roh MS, Homer RJ, et al. POU2F3 in SCLC: Clinicopathologic and genomic analysis with a focus on its diagnostic utility in Neuroendocrine-Low SCLC. J Thorac Oncol. 2022;17(9):1109–21.
34. Meuwissen R, Linn SC, Linnoila RI, Zevenhoven J, Mooi WJ, Berns A. Induction of small cell lung cancer by somatic inactivation of both Trp53 and Rb1 in a conditional mouse model. Cancer Cell. 2003;4(3):181–9.
35. Dupage M, Dooley AL, Jacks T. Conditional mouse lung cancer models using adenoviral or lentiviral delivery of cre recombinase. Nat Protoc. 2009;4(7):1064–72.

Publisher's note

Springer Nature remains neutral with regard to jurisdictional claims in published maps and institutional affiliations.